A VARIABLE SAMPLE SIZE SYNTHETIC CHART FOR THE COEFFICIENT OF VARIATION

M. Yahaya[1], S.L. Lim[1*], A.I.N. Ibrahim[1], W.C. Yeong[2] & M.B.C. Khoo[3]

ARTICLE INFO

Article details
Submitted by authors 26 Jun 2021
Accepted for publication 15 Nov 2021
Available online 06 May 2022

Contact details
* Corresponding author
sokli@um.edu.my

Author affiliations
1 Institute of Mathematical Sciences, Faculty of Science, Universiti Malaya, 50603 Kuala Lumpur, Malaysia

2 Department of Operations and Management Information Systems, Faculty of Business and Accountancy, Universiti Malaya, 50603 Kuala Lumpur, Malaysia

3 School of Mathematical Sciences, Universiti Sains Malaysia, 11800, Penang, Malaysia

ORCID® identifiers
M. Yahaya
0000-0003-1426-7630

S.L. Lim
0000-0003-3554-6874

A.I.N. Ibrahim
0000-0003-4174-6434

W.C. Yeong
0000-0002-0579-6621

M.B.C. Khoo
0000-0002-3245-1127

DOI
http://dx.doi.org/10.7166/33-1-2545

ABSTRACT

A variable sample size (VSS) synthetic chart to monitor the coefficient of variation (γ) is proposed in this paper to improve the performance of the existing synthetic γ chart. A description of how the chart operates, as well as the formulae for various performance measures (i.e., the average run length (*ARL*), standard deviation of the run length (*SDRL*), average sample size (*ASS*), and expected average run length (*EARL*)) are proposed. The algorithms that optimise the out-of-control *ARL* (ARL_1) and *EARL* ($EARL_1$), subject to the constraints in the in-control *ARL* (ARL_0) and *ASS* (ASS_0), are also proposed. Subsequently, optimal charting parameters for various numerical examples are obtained. The proposed chart shows a significant improvement over the existing synthetic γ-chart. Comparisons with other γ-charts also show that the proposed chart performs better than the Shewhart-γ and VSS-γ charts under all cases, while showing better performance than the exponentially weighted moving average (EWMA) and VSS EWMA-γ^2 charts for moderate and large shift sizes. Finally, this paper shows the implementation of the proposed chart on an actual industrial example.

OPSOMMING

'n Veranderlike Steekproefgrootte sintetiese grafiek om die variasiekoëffisiënt (γ) te monitor, word in hierdie artikel voorgestel om die werkverrigting van die bestaande sintetiese grafiek te verbeter. 'n Beskrywing van hoe die grafiek werk, sowel as die formules vir verskeie prestasiemaatstawwe (d.w.s. die gemiddelde lopielengte, standaardafwyking van die lopielengte, gemiddelde steekproefgrootte en verwagte gemiddelde lopielengte) word voorgestel. Die algoritmes wat die buite-beheer gemiddelde lopielengte) en verwagte gemiddelde lopielengte optimeer, onderhewig aan die beperkings in die in-beheer gemiddelde lopielengte en gemiddelde steekproefgrootte, word ook voorgestel. Vervolgens word optimale parameters vir verskeie numeriese voorbeelde verkry. Die voorgestelde grafiek toon 'n aansienlike verbetering teenoor die bestaande sintetiese γ grafiek. Vergelykings met ander γ-grafieke toon ook dat die voorgestelde grafiek beter presteer as die Shewhart-γ en Veranderlike Steekproefgrootte-γ^2 kaarte onder alle gevalle, terwyl dit beter prestasie toon as die eksponensieel geweegde bewegende gemiddelde γ^2 kaarte vir matige en groot skofgroottes. Ten slotte, hierdie artikel toon die implementering van die voorgestelde grafiek op 'n werklike voorbeeld in die industrie.

1 INTRODUCTION

By convention, most control charts monitor changes in the mean (μ) and/or standard deviation (σ) – for example, Coelho, Chakraborti and Graham [1], Teoh, Fun, Khoo and Yeong [2], and many others. However,

not all processes have a constant μ. In addition, σ may change according to μ. One of the reasons this may happen is changes in process outputs as a result of different planning decisions, or it may be due to the inherent properties of the process. Dubious conclusions will be reached if such processes are monitored through conventional $\bar{X}$ and *R* or *S* charts, since shifts in μ and/or σ do not mean that the process is out of control (OOC).

A chart monitoring the coefficient of variation (γ) was first proposed by Kang, Lee, Seong and Hawkins [3], where $\gamma = \frac{\sigma}{\mu}$. For this type of chart, an OOC condition is only signalled with a change in the relationship between σ and μ. In other words, as long as $\frac{\sigma}{\mu}$ does not shift from the in-control (IC) value of γ, the process is IC. Yeong, Khoo, Tham, Teoh and Rahim [4] have reviewed several areas of application when monitoring γ is important.

Numerous new charts are proposed to monitor γ, one of which is the synthetic chart by Calzada and Scariano [5]. The synthetic chart produces an OOC signal if successive samples falling outside the control limits are close to each other. It is preferred by practitioners, as it is easy to understand and implement, and is free from the inertia effect faced by the exponentially weighted moving average (EWMA) chart. The synthetic-γ chart outperforms the γ-chart by Kang *et al.* [3], but is inferior to the EWMA chart proposed by Castagliola, Celano and Psarakis [6]. Thus this paper will improve the performance of the synthetic-γ chart by introducing the variable sample size (VSS) scheme into the synthetic-γ chart.

The VSS feature is an adaptive feature in which charting parameters are varied according to the most recent sample information. The adaptive feature was recently incorporated into charts monitoring γ. Castagliola, Achouri, Taleb, Celano and Psarakis [7] first proposed the variable sampling interval (VSI)-γ chart. Later, Castagliola, Achouri, Taleb, Celano and Psarakis [8] proposed variable sample size (VSS)-γ charts. Subsequently, Khaw, Khoo, Yeong and Wu [9] and Yeong, Lim, Khoo and Castagliola [10] proposed the variable sample size and sampling interval (VSSI) and the variable parameters (VP)-γ charts respectively. [7] to [9] incorporated adaptive features into the simpler Shewhart-type γ charts. This encouraged Yeong *et al.* [4] and Anis, Yeong, Chong, Lim and Khoo [11] to incorporate the VSI and VSS features respectively, into more complicated charts, such as the EWMA charts. From these studies, adapting the charting parameters according to the most recent sample information results in a significant improvement.

No studies are available in the literature on adaptive-type synthetic-γ charts. The synthetic-γ charts are attractive to practitioners, as they wait until two successive samples fall outside the control limits before deciding whether the process is IC or OOC, unlike Shewhart-type γ charts, which immediately send OOC signals when a sample falls outside the control limits. Thus this paper will propose a VSS synthetic-γ chart, which is expected to improve the performance of the existing synthetic-γ chart. This paper is organised as follows: Section 2 reviews the existing synthetic-γ chart and describes the transformed statistics (T_i) that will be adopted in this paper. Then Section 3 introduces the proposed VSS synthetic-γ chart and the formulae to evaluate various performance measures. Next, Section 4 proposes the algorithm to obtain the optimal charting parameters, and shows the optimal performance of the proposed chart based on numerical examples. Section 5 compares the performance of the proposed chart with other γ charts, while the proposed chart is implemented on an actual industrial example in Section 6. Finally, the conclusion is provided in Section 7.

2 THE SYNTHETIC-γ CHART AND TRANSFORMED STATISTICS (TI)

The synthetic-γ chart is made up of two sub-charts — i.e., the γ and conforming run length (*CRL*) sub-charts. In the γ sub-chart, if $\hat{\gamma} < LCL$ or $\hat{\gamma} > UCL$ (where $\hat{\gamma}, LCL$ and UCL are the sample γ, lower control limit and upper control limit respectively), the sample is a non-conforming sample; conversely, if $\hat{\gamma}$ falls between the *LCL* and *UCL*, it is a conforming sample. The *CRL* sub-chart defines the number of conforming samples between successive non-conforming samples (including the ending non-conforming sample) as the *CRL*. If $CRL \leq L$, where *L* is a pre-determined threshold, then the process is considered to be OOC.

The *LCL* and *UCL* of the γ sub-chart are computed as

$$LCL = \mu_0(\hat{\gamma}) - K\sigma_0(\hat{\gamma}), \tag{1}$$

and

$$UCL = \mu_0(\hat{\gamma}) + K\sigma_0(\hat{\gamma}), \tag{2}$$

where *K* represents the control limit coefficient, while $\mu_0(\hat{\gamma})$ and $\sigma_0(\hat{\gamma})$ are the IC mean and standard deviation of $\hat{\gamma}$ respectively. Reh and Scheffler [12] approximated $\mu_0(\hat{\gamma})$ and $\sigma_0(\hat{\gamma})$ as

$$\mu_0(\hat{\gamma}) \approx \gamma_0\left[1+\frac{1}{n}\left(\gamma_0^2-\frac{1}{4}\right)+\frac{1}{n^2}\left(3\gamma_0^4-\frac{\gamma_0^2}{4}-\frac{7}{32}\right)+\frac{1}{n^3}\left(15\gamma_0^6-\frac{3\gamma_0^4}{4}-\frac{7\gamma_0^2}{32}-\frac{19}{128}\right)\right] \tag{3}$$

and

$$\sigma_0(\hat{\gamma}) \approx \gamma_0\sqrt{\frac{1}{n}\left(\gamma_0^2+\frac{1}{2}\right)+\frac{1}{n^2}\left(8\gamma_0^4+\gamma_0^2+\frac{3}{8}\right)+\frac{1}{n^3}\left(69\gamma_0^6+\frac{7\gamma_0^4}{2}+\frac{3\gamma_0^2}{4}+\frac{3}{16}\right)}, \tag{4}$$

where γ_0 and *n* are the IC γ and sample size respectively.

Note that the *LCL* and *UCL* are functions of *n*. For the existing synthetic-γ chart, which adopts fixed sample sizes, there is only one pair of (*LCL*, *UCL*). However, if variable sample sizes are adopted — for example, small and large sample sizes (n_S and n_L) — there will be a pair of (*LCL*, *UCL*) for n_S and another pair of (*LCL*, *UCL*) for n_L. In addition, VSS charts involve lower and upper warning limits (*LWL* and *UWL*) to establish the warning region, where, similar to the *LCL* and *UCL*, they are also functions of *n*. Thus, if two levels of sample sizes are adopted (n_S and n_L), there will be two pairs of (*LCL*, *UCL*) and two pairs of (*LWL*, *UWL*) — i.e., one pair of (*LCL*, *UCL*) and (*LWL*, *UWL*) for n_S, and another pair of (*LCL*, *UCL*) and (*LWL*, *UWL*) for n_L. Furthermore, both the warning and the control limits are asymmetric limits. This results in a significant increase in the computational effort to design the chart because of the larger number of charting parameters. It also results in a difficulty during implementation and interpretation, as the samples need to be plotted against different pairs of limits [8].

Thus the approach by Castagliola *et al*. [8] is adopted: instead of directly monitoring $\hat{\gamma}$ of the *i*th subgroup $(\hat{\gamma}_i)$, the transformed statistics T_i are monitored instead. The statistics T_i are defined as

$$T_i = a + b\ln(\hat{\gamma}_i - c), \tag{5}$$

where $a,b>0$ and *c* are parameters that depend on $n(i)$ and γ_0. Here, $n(i)$ is the sample size of the *i*th subgroup. The parameters (a,b,c) can be estimated as

$$b = \frac{F_N^{-1}(r)}{\ln\left(\frac{x_{0.5}-x_r}{x_{1-r}-x_{0.5}}\right)}, \tag{6}$$

$$a = -b\ln\left(\frac{x_{0.5}-x_r}{1-\exp\left(\frac{F_N^{-1}(r)}{b}\right)}\right), \tag{7}$$

and

$$c = x_{0.5} - e^{-\frac{a}{b}}, \tag{8}$$

where $x_r = F_{\hat{\gamma}}^{-1}\left(r\middle|n(i),\gamma_0\right), x_{0.5} = F_{\hat{\gamma}}^{-1}\left(0.5\middle|n(i),\gamma_0\right)$, $x_{1-r} = F_{\hat{\gamma}}^{-1}\left(1-r\middle|n(i),\gamma_0\right)$ are the quantiles for the distribution of $\hat{\gamma}$, and $F_N^{-1}(r)$ is the inverse standard normal distribution. Note that $F_{\hat{\gamma}}^{-1}(.)$ is the inverse

cumulative distribution function (cdf) of $\hat{\gamma}$, where $F_{\hat{\gamma}}^{-1}\left(\alpha|n(i),\gamma_0\right)=\dfrac{\sqrt{n}}{F_t^{-1}\left(1-\alpha\left|n-1,\dfrac{\sqrt{n(i)}}{\gamma_0}\right.\right)}$, with $F_t^{-1}(.)$ being the inverse cdf of the non-central *t* distribution.

Castagliola *et al*. [8] have shown that, for $r\in[0.01,0.1]$, the T_i statistics are well approximated by a standard normal distribution, as $r\geq 0.01$ will avoid giving too much weight to the tails of the $\hat{\gamma}$ distribution, while $r\leq 0.1$ will capture enough information from the tails. Through simulations, Castagliola *et al*. [8] have shown that the T_i statistics follow the standard normal distribution for $r\in[0.01,0.1]$. This is achieved by simulating a large number of $\hat{\gamma}$ from different values of *n* and γ_0, computing the T_i statistics based on different *r* values between 0.01 and 0.1, and performing an Anderson-Darling test to show that the T_i statistics follow a standard normal distribution for all values of *r* within that range. In this paper, as in that of Castagliola *et al*. [8], the intermediate value of $r=0.05$ is adopted. However, practitioners can also choose other values of $r\in[0.01,0.1]$ for the T_i statistics to follow the standard normal distribution; hence any value of $r\in[0.01,0.1]$ will not have an impact. Note that the T_i statistics are only approximated well by a standard normal distribution if the observations of the quality characteristic being monitored are independent and identically distributed normal variates.

3 THE VARIABLE SAMPLE SIZE (VSS) SYNTHETIC-γ CHART

The proposed chart works in a similar way to the existing synthetic-γ chart, except that the sample size is varied at two levels, as shown in Figure 1.

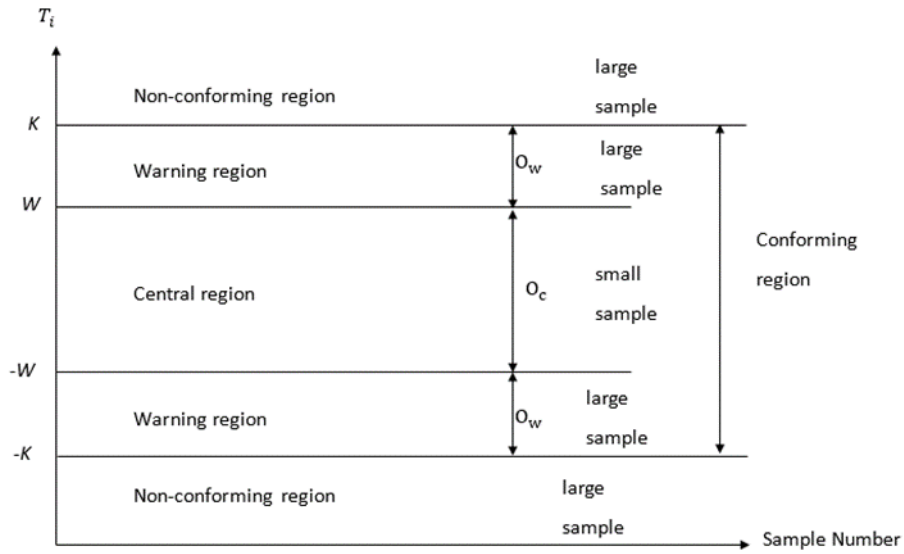

Figure 1: The γ sub-chart of the VSS synthetic γ chart

Figure 1 shows that the conforming region is separated into the central and warning regions. When $-W\leq T_i\leq W$, the sample belongs to the central conforming region, while when $W<T_i<K$ or $-K<T_i<-W$, the sample falls in the warning conforming region. When $T_i>K$ or $T_i<-K$, the sample is non-conforming. The samples that fall in the central conforming, warning conforming, and non-conforming regions are denoted as $0_C, 0_W$ and 1 respectively.

The sample size $n(i)$ of the i^{th} subgroup depends on the region in which T_{i-1} falls. If T_{i-1} falls in the central conforming region, then $n(i)=n_S$; but if T_{i-1} falls in the warning conforming region or the non-conforming region, then $n(i)=n_L$.

Let

$$A^+ = P\left(-W < T_i < W \middle| n_S, \gamma\right), \tag{9}$$

$$A^- = P\left(-W < T_i < W \middle| n_L, \gamma\right), \tag{10}$$

$$B^+ = P\left(\left(-K < T_i < -W\right) \cup \left(W < T_i < K\right) \middle| n_S, \gamma\right), \tag{11}$$

$$B^- = P\left(\left(-K < T_i < -W\right) \cup \left(W < T_i < K\right) \middle| n_L, \gamma\right), \tag{12}$$

$$C^+ = P\left(\left(T_i < -K\right) \cup \left(T_i > K\right) \middle| n_S, \gamma\right), \tag{13}$$

$$C^- = P\left(\left(T_i < -K\right) \cup \left(T_i > K\right) \middle| n_L, \gamma\right). \tag{14}$$

The probability A^+ is obtained as follows:

$$\begin{aligned} A^+ &= P\left(-W < T_i < W \middle| n_S, \gamma\right) \\ &= P\left(-W < a + b\ln\left(\hat{\gamma}_i - c\right) < W \middle| n_s, \gamma\right) \\ &= F_{\hat{\gamma}}\left(\exp\left(\frac{W-a}{b}\right) + c \middle| n_S, \gamma\right) - F_{\hat{\gamma}}\left(\exp\left(\frac{-W-a}{b}\right) + c \middle| n_S, \gamma\right) \\ &= F_t\left(\frac{\sqrt{n_S}}{\exp\left(\frac{-W-a}{b}\right)} + c \middle| n_S - 1, \frac{\sqrt{n_S}}{\gamma}\right) - F_t\left(\frac{\sqrt{n_S}}{\exp\left(\frac{W-a}{b}\right)} + c \middle| n_S - 1, \frac{\sqrt{n_S}}{\gamma}\right) \end{aligned} \tag{15}$$

where $F_{\hat{\gamma}}(.)$ is the cdf of $\hat{\gamma}$ and $F_t(.)$ is the cdf of the non-central *t* distribution. Castagliola *et al*. [6] have shown that $F_{\hat{\gamma}}\left(x \middle| n, \gamma\right) = 1 - F_t\left(\frac{\sqrt{n}}{x} \middle| n-1, \frac{\sqrt{n}}{\gamma}\right)$.

Similarly, the probabilities A^-, B^+, B^-, C^+, C^- can be obtained as follows:

$$A^- = F_t\left(\frac{\sqrt{n_L}}{\exp\left(\frac{-W-a}{b}\right)} + c \middle| n_L - 1, \frac{\sqrt{n_L}}{\gamma}\right) - F_t\left(\frac{\sqrt{n_L}}{\exp\left(\frac{W-a}{b}\right)} + c \middle| n_L - 1, \frac{\sqrt{n_L}}{\gamma}\right), \tag{16}$$

$$B^+ = F_t\left(\frac{\sqrt{n_S}}{\exp\left(\frac{-K-a}{b}\right)} + c \middle| n_S - 1, \frac{\sqrt{n_S}}{\gamma}\right) - F_t\left(\frac{\sqrt{n_S}}{\exp\left(\frac{-W-a}{b}\right)} + c \middle| n_S - 1, \frac{\sqrt{n_S}}{\gamma}\right) + F_t\left(\frac{\sqrt{n_S}}{\exp\left(\frac{W-a}{b}\right)} + c \middle| n_S - 1, \frac{\sqrt{n_S}}{\gamma}\right) - F_t\left(\frac{\sqrt{n_S}}{\exp\left(\frac{K-a}{b}\right)} + c \middle| n_S - 1, \frac{\sqrt{n_S}}{\gamma}\right), \tag{17}$$

$$B^- = F_t\left(\frac{\sqrt{n_L}}{\exp\left(\frac{-K-a}{b}\right)} + c \middle| n_L - 1, \frac{\sqrt{n_L}}{\gamma}\right) - F_t\left(\frac{\sqrt{n_L}}{\exp\left(\frac{-W-a}{b}\right)} + c \middle| n_L - 1, \frac{\sqrt{n_L}}{\gamma}\right) + F_t\left(\frac{\sqrt{n_L}}{\exp\left(\frac{W-a}{b}\right)} + c \middle| n_L - 1, \frac{\sqrt{n_L}}{\gamma}\right) - F_t\left(\frac{\sqrt{n_L}}{\exp\left(\frac{K-a}{b}\right)} + c \middle| n_L - 1, \frac{\sqrt{n_L}}{\gamma}\right), \tag{18}$$

$$C^+ = 1 - F_t\left(\frac{\sqrt{n_S}}{\exp\left(\frac{-K-a}{b}\right)} + c \middle| n_S - 1, \frac{\sqrt{n_S}}{\gamma}\right) + F_t\left(\frac{\sqrt{n_S}}{\exp\left(\frac{K-a}{b}\right)} + c \middle| n_S - 1, \frac{\sqrt{n_S}}{\gamma}\right), \tag{19}$$

$$C^- = 1 - F_t\left(\frac{\sqrt{n_L}}{\exp\left(\frac{-K-a}{b}\right)} + c \middle| n_L - 1, \frac{\sqrt{n_L}}{\gamma}\right) + F_t\left(\frac{\sqrt{n_L}}{\exp\left(\frac{K-a}{b}\right)} + c \middle| n_L - 1, \frac{\sqrt{n_L}}{\gamma}\right). \tag{20}$$

The formulae for the average run length (*ARL*), standard deviation of the run length (*SDRL*), expected average run length (*EARL*), and average sample size (*ASS*) will be developed using a Markov chain approach. The states of the Markov chain are defined based on *L* consecutive samples; thus there will be a total of

$(2L+1)$ IC states that are transient and one OOC absorbing state. The OOC absorbing state refers to the state where $CRL \le L$.

For *L* = 2, the transient states are defined as

State 1: 00_C
State 2: 00_W
State 3: 01
State 4: 10_C
State 5: 10_W,

where 0 denotes the conforming region, while State 6 will be the absorbing state. For $L \ge 3$, the transient states are defined as

State 1 : $00...00...00_C$
State 2 : $00...00...00_W$
State 3 : $00...00...01$
State 4 : $00...00...10_C$
State 5 : $00...00...10_W$
$\vdots$
State $2L$: $10...00..00_C$
State $(2L+1)$: $10...00..00_W$,

while State $(2L+2)$ will be the absorbing state.

A $(2L+1)\times(2L+1)$ matrix that consists of the transition probabilities among the transient states, as defined in the previous paragraph, can be obtained. This transition probability matrix is denoted as $\mathbf{Q}$. For $L=2$, $\mathbf{Q}$ can be obtained as follows:

$$\mathbf{Q} = \begin{pmatrix} A^+ & B^+ & C^+ & 0 & 0 \\ A^- & B^- & C^- & 0 & 0 \\ 0 & 0 & 0 & A^- & B^- \\ A^+ & B^+ & 0 & 0 & 0 \\ A^- & B^- & 0 & 0 & 0 \end{pmatrix}. \tag{21}$$

For $L \ge 3$, $\mathbf{Q}$ is a $(2L+1)\times(2L+1)$ matrix with all elements zero, except:

1. For the first row, $Q(1,1)=A^+, Q(1,2)=B^+, Q(1,3)=C^+$.
2. For the second row, $Q(2,1)=A^-, Q(2,2)=B^-, Q(2,3)=C^-$.
3. For the third row, $Q(3,4)=A^-, Q(3,5)=B^-$.
4. For rows *i*, where $i=4,...,(2L-1)$, if *i* is even, $Q(i,i+2)=A^+, Q(i,i+3)=B^+$, while if *i* is odd, $Q(i,i+1)=A^-, Q(i,i+2)=B^-$.
5. For row $(2L)$, $Q(2L,1)=A^+, Q(2L,2)=B^+$.
6. For row $(2L+1)$, $Q(2L+1,1)=A^-, Q(2L+1,2)=B^-$.

The transition probability matrix can then be obtained as follows:

$$\mathbf{P} = \begin{pmatrix} \mathbf{Q} & \mathbf{r} \\ \mathbf{0} & 1 \end{pmatrix}, \tag{22}$$

where $\mathbf{Q}$ is the $(2L+1)\times(2L+1)$ matrix as shown in the preceding paragraph, $\mathbf{r} = \mathbf{1} - \mathbf{Q1}$ with $\mathbf{1}$ being a $(2L+1)\times 1$ vector of ones, and $\mathbf{0}$ is a $1\times(2L+1)$ vector of zeros. Note that state $(2L+2)$ of $\mathbf{P}$ in (14) is the OOC state.

The *ARL* and *SDRL* can then be computed as

$$ARL = \mathbf{q}^T (\mathbf{I} - \mathbf{Q})^{-1} \mathbf{1} \tag{23}$$

and

$$SDRL = \sqrt{2\mathbf{q}^T (\mathbf{I} - \mathbf{Q})^{-2} \mathbf{Q}\mathbf{1} - ARL^2 + ARL}, \tag{24}$$

where $\mathbf{q}$ is the $(2L+1)\times 1$ vector of initial probabilities for the transient states, $\mathbf{I}$ is the $(2L+1)\times(2L+1)$ identity matrix, and $\mathbf{1}$ is a $(2L+1)\times 1$ vector of ones. For a zero-state condition, except for the 3rd element of $\mathbf{q}$ which is one, all other elements are zeros. This paper will design the proposed chart based on the zero-state condition.

To calculate the OOC *ARL* (ARL_1) and OOC *SDRL* ($SDRL_1$), $\gamma = \gamma_1 = \tau\gamma_0$ ($\tau > 1$) is substituted into Equations (15) to (20), where γ_1 is the OOC γ and τ is the shift size, to obtain the OOC $\mathbf{Q}$ from Equation (21). To compute the IC *ARL* (ARL_0) and *SDRL* ($SDRL_0$), $\gamma = \gamma_0$ is substituted into Equations (15) to (20) to obtain the OOC $\mathbf{Q}$ from Equation (21). The ARL_1 and $SDRL_1$ are then calculated by substituting the OOC $\mathbf{Q}$ into Equations (23) and (24) respectively, while ARL_0 and $SDRL_0$ are calculated by substituting the IC $\mathbf{Q}$ into Equations (23) and (24) respectively.

The exact value of τ is not always known, and without knowing its exact value, the ARL_1 cannot be computed. For this scenario, the *EARL* will be adopted as a performance measure. The *EARL* does not require the shift size to be estimated as an exact value; instead, it only needs to be estimated as a range $(\tau_{\min}, \tau_{\max})$.

The following shows the computation of the *EARL*:

$$EARL = \int_{\tau_{\min}}^{\tau_{\max}} f_\tau(\tau) ARL(\tau, \gamma_0, n_S, n_L, W, K) d\tau, \tag{25}$$

where $f_\tau(\tau)$ is the probability density function (pdf) of τ. As in the study of Castagliola *et al.* [6], τ is assumed to be uniformly distributed over $(\tau_{\min}, \tau_{\max})$. The integral cannot be obtained analytically; thus the Gauss-Legendre quadrature is adopted to solve the integral.

Subsequently, the formula for the *ASS* will be shown. The *ASS* needs to be evaluated so that the IC *ASS* (ASS_0) can be maintained at a specific value, especially when the cost of sampling is of concern to the practitioner.

The formula for the *ASS* is developed through a Markov chain approach, as proposed by Castagliola *et al.* [8]. First, $\mathbf{P}$ in Equation (22) is transformed into a similar matrix $\mathbf{P}^*$, where

$$\mathbf{P}^* = \begin{pmatrix} \mathbf{Q} & \mathbf{r} \\ \mathbf{q}^T & 0 \end{pmatrix}. \tag{26}$$

From $\mathbf{P}^*$, once the process reaches the OOC state (State $(2L+2)$), the process will restart at State 3.

Let $\boldsymbol{\pi} = (\pi_0, \ \pi_1, \ \ldots \ \pi_{2L+2})^T$ be the stationary probability vector of $\mathbf{P}^*$, where π_j is the stationary probability for the process to fall in the j^{th} state, where $j = 0,1,\ldots,2L+2$. $\boldsymbol{\pi}$ can be computed as follows:

$$\boldsymbol{\pi} = \mathbf{R}^{-1} \begin{pmatrix} \mathbf{q} \\ 0 \end{pmatrix}, \tag{27}$$

where the matrix $\mathbf{R}$ is obtained by deducting 1 from the diagonal elements of the transpose of $\mathbf{P}^*$; then replace the third row of this matrix with ones.

The *ASS* is then computed as

$$ASS = (n_S \quad n_L \quad n_L \quad n_S \quad n_L \quad \cdots \quad \cdots \quad n_S \quad n_L)\boldsymbol{\pi}. \tag{28}$$

4 NUMERICAL EXAMPLES

This section shows the algorithms to obtain the optimal charting parameters $\left(L^*, n_S^*, n_L^*, W^*, K^*\right)$. Next, the optimal charting parameters *ARL*$_1$ and *SDRL*$_1$ for the numerical examples with different values of γ_0, n and τ are shown. Furthermore, the optimal charting parameters and *EARL*$_1$ for different γ_0 and n are also shown for the case when τ could not be specified.

Two algorithms are proposed. In the first algorithm, $\left(L^*, n_S^*, n_L^*, W^*, K^*\right)$ is chosen to minimise *ARL*$_1$, subject to constraints in *ARL*$_0$ and *ASS*$_0$. In the second algorithm, $\left(L^*, n_S^*, n_L^*, W^*, K^*\right)$ is chosen to minimise the *EARL* instead, subject to constraints in *ARL*$_0$ and *ASS*$_0$.

The following are the steps to implement the first algorithm:

1. Specify the values of *n*, γ_0, *ARL*$_0$ and τ.
2. Set *L* = 1.
3. Set $n_S = 2$.
4. Set $n_L = n+1$, where *n* is the sample size.
5. Obtain (W, K) so that $ARL_0 = \xi$ and *ASS*$_0$ = *n*, by solving Equations (23) and (28) with $\gamma = \gamma_0$. Note that ξ is determined by the practitioner.
6. With the current combination of $\left(L, n_S, n_L, W, K\right)$, compute *ARL*$_1$ and *SDRL*$_1$ from Equations (23) and (24) respectively, with $\gamma = \tau\gamma_0$.
7. Increase n_L by 1.
8. Repeat Steps 5 to 7 until $n_L = n_{\max}$, where $n_{\max}$ is determined by the practitioner based on the availability of resources. In this paper, $n_{\max} = 31.$
9. Increase n_S by 1.
10. Repeat Steps 4 to 9 until $n_S = n-1$.
11. Increase *L* by 1.
12. Repeat Steps 3 to 11 until the *ARL*$_1$ for *L*+1 is larger than the *ARL*$_1$ for *L*.
13. The combination with the smallest *ARL*$_1$ is the optimal charting parameters $\left(L^*, n_S^*, n_L^*, W^*, K^*\right)$.

In the second algorithm, $\left(L^*, n_S^*, n_L^*, W^*, K^*\right)$ is chosen to minimise the *EARL* instead. The steps to obtain $\left(L^*, n_S^*, n_L^*, W^*, K^*\right)$ are similar to Steps 1 to 13 in the preceding paragraph, with modifications made for the following steps:

1. Specify the values of *n*, γ_0, *ARL*$_0$, $\tau_{\min}$ and $\tau_{\max}$.
6. With the current combination of $\left(L, n_S, n_L, W, K\right)$, compute *EARL*$_1$ from Equation (25).
13. The combination with the smallest *EARL*$_1$ is the optimal charting parameters $\left(L^*, n_S^*, n_L^*, W^*, K^*\right)$.

Table 1 shows the $\left(L^*, n_S^*, n_L^*, W^*, K^*\right)$, *ARL*$_1$ and *SDRL*$_1$ values for $n \in \{5, 7, 10, 15\}$, $\tau \in \{1.1, 1.2, 1.5, 2.0\}$ and $\gamma_0 \in \{0.05, 0.10, 0.15, 0.20\}$. The *ARL*$_0$ is set as 370.4. To interpret Table 1, we refer to the combination $\gamma_0 = 0.05, n = 5$ and $\tau = 1.1$, which shows that $\left(L^*, n_S^*, n_L^*, W^*, K^*\right) = (28, 2, 30, 1.60, 2.19)$, with *ARL*$_1$ = 68.92 and *SDRL*$_1$ = 92.75.

From Table 1, most of the optimal charting parameters show a large difference between n_S^* and n_L^*, where all the $n_S^* = 2$, while most of the n_L^* are equivalent or close to $n_{\max}$. A larger *n* results in smaller *ARL*$_1$ and *SDRL*$_1$ values. For example, for $\gamma_0 = 0.05$ and $\tau = 1.1$, $(ARL_1, SDRL_1) = (68.92, 92.75)$ when *n* = 5, while $(ARL_1, SDRL_1) = (36.64, 48.39)$ when *n* = 15. Thus a larger *n* results in a better performance. The improvement

is more significant when τ is small. A smaller *W* and a larger *K* are also observed for a larger *n*, which translates into a larger warning region but a smaller conforming region.

Similar to *n*, smaller ARL_1 and $SDRL_1$ are observed for larger τ, since a larger shift requires fewer samples to detect the shift. A larger τ also results in smaller *L* and *K*. This shows that a smaller conforming region is adopted; but successive non-conforming samples should happen quite close to each other for the process to be considered as OOC. A larger γ_0 results in a slight increase in the ARL_1 and $SDRL_1$, especially for small shift sizes.

Table 1: The $\left(L^*, n_S^*, n_L^*, W^*, K^*\right)$ and the corresponding ARL_1 and $SDRL_1$ for the VSS synthetic-γ chart

τ	$\gamma_0 = 0.05$	$\gamma_0 = 0.10$	$\gamma_0 = 0.15$	$\gamma_0 = 0.20$
$n=5$				
1.1	(28, 2, 30, 1.60, 2.19) (68.92, 92.75)	(30, 2, 31, 1.61, 2.22) (69.71, 93.85)	(25, 2, 30, 1.61, 2.19) (70.63, 94.56)	(28, 2, 28, 1.55, 2.23) (72.89, 97.26)
1.2	(13, 2, 31, 1.59, 2.10) (14.34, 21.27)	(19, 2, 30, 1.59, 2.16) (14.65, 21.29)	(17, 2, 29, 1.57, 2.15) (15.47, 22.39)	(20, 2, 31, 1.64, 2.17) (16.84, 24.53)
1.5	(6, 2, 31, 1.64, 2.00) (1.47, 2.00)	(9, 2, 31, 1.64, 2.05) (1.49, 2.01)	(9, 3, 31, 1.71, 2.20) (1.54, 1.90)	(8, 2, 31, 1.64, 2.05) (1.62, 2.28)
2.0	(4, 2, 31, 1.64, 1.95) (1.00, 0.11)	(3, 2, 31, 1.64, 1.91) (1.00, 0.12)	(3, 2, 31, 1.64, 1.92) (1.00, 0.15)	(5, 2, 31, 1.64, 1.99) (1.01, 0.17)
$n=7$				
1.1	(29, 2, 31, 1.44, 2.23) (57.57, 77.59)	(30, 2, 31, 1.44, 2.24) (58.30, 78.54)	(29, 2, 31, 1.42, 2.25) (58.97, 79.25)	(29, 2, 31, 1.43, 2.26) (62.11, 83.28)
1.2	(20, 2, 31, 1.41, 2.19) (10.62, 14.72)	(19, 2, 30, 1.39, 2.19) (10.99, 15.20)	(19, 2, 31, 1.43, 2.19) (11.69, 16.37)	(17, 2, 31, 1.41, 2.19) (12.09, 16.96)
1.5	(6, 2, 31, 1.44, 2.02) (1.32, 1.33)	(6, 2, 31, 1.44, 2.03) (1.34, 1.38)	(6, 2, 31, 1.44, 2.03) (1.38, 1.46)	(6, 2, 31, 1.43, 2.04) (1.43, 1.56)
2.0	(3, 2, 31, 1.44, 1.93) (1.00, 0.08)	(3, 2, 31, 1.44, 1.93) (1.00, 0.09)	(4, 2, 31, 1.44, 1.98) (1.00, 0.10)	(3, 2, 31, 1.43, 1.94) (1.00, 0.13)
$n=10$				
1.1	(29, 2, 31, 1.17, 2.28) (45.81, 61.37)	(30, 2, 31, 1.18, 2.29) (47.15, 63.17)	(27, 2, 31, 1.18, 2.28) (48.89, 65.37)	(30, 2, 31, 1.17, 2.31) (50.58, 67.58)
1.2	(12, 2, 31, 1.16, 2.16) (8.11, 10.96)	(19, 2, 31, 1.18, 2.23) (8.36, 10.79)	(11, 2, 31, 1.15, 2.16) (8.71, 11.86)	(20, 2, 31, 1.17, 2.25) (9.24, 11.91)
1.5	(4, 2, 31, 1.18, 2.00) (1.23, 0.91)	(4, 2, 31, 1.18, 2.01) (1.24, 0.94)	(3, 2, 31, 1.18, 1.97) (1.27, 1.04)	(4, 2, 31, 1.17, 2.02) (1.31, 1.08)
2.0	(2, 2, 31, 1.17, 1.91) (1.00, 0.06)	(2, 2, 31, 1.16, 1.91) (1.00, 0.06)	(2, 2, 31, 1.17, 1.91) (1.00, 0.08)	(2, 2, 31, 1.17, 1.92) (1.00, 0.09)
$n=15$				
1.1	(30, 2, 31, 0.82, 2.36) (36.64, 48.39)	(29, 2, 31, 0.82, 2.36) (37.49, 49.56)	(30, 2, 31, 0.82, 2.37) (38.74, 51.20)	(28, 2, 31, 0.82, 2.37) (40.82, 54.00)
1.2	(12, 2, 31, 0.82, 2.23) (6.25, 7.67)	(12, 2, 31, 0.82, 2.23) (6.41, 7.89)	(13, 2, 31, 0.82, 2.25) (6.68, 8.18)	(18, 2, 31, 0.82, 2.30) (7.12, 8.36)
1.5	(3, 2, 31, 0.82, 2.02) (1.18, 0.63)	(4, 2, 31, 0.82, 2.06) (1.19, 0.63)	(3, 2, 31, 0.82, 2.02) (1.21, 0.70)	(5, 2, 31, 0.82, 2.10) (1.24, 0.70)
2.0	(2, 2, 31, 0.82, 1.95) (1.00, 0.04)	(2, 3, 31, 0.82, 2.04) (1.00, 0.05)	(2, 2, 31, 0.82, 1.96) (1.00, 0.06)	(2, 2, 31, 0.82, 1.96) (1.00, 0.07)

Table 2 shows the $\left(L^*, n_S^*, n_L^*, W^*, K^*\right)$ and $EARL_1$ values for $n \in \{5,7,10,15\}$, $\gamma_0 \in \{0.05, 0.10, 0.15, 0.20\}$ and $(\tau_{\min}, \tau_{\max}) = (1,2]$ by using the second algorithm. Similar to Table 1, the ARL_0 is set as 370.4. For instance, for $(\tau_{\min}, \tau_{\max}) = (1,2]$, $\gamma_0 = 0.05$ and $n = 5$, $\left(L^*, n_S^*, n_L^*, W^*, K^*\right) = (28, 2, 30, 1.60, 2.19)$, with $EARL_1 = 15.39$.

Table 2: The $\left(L^*, n_S^*, n_L^*, W^*, K^*\right)$ and the corresponding *EARL*$_1$ for the VSS synthetic-γ chart

γ_0	L^*	n_S^*	n_L^*	W^*	K^*	*EARL*$_1$
$n=5$						
0.05	28	2	30	1.60	2.19	15.39
0.10	25	2	30	1.61	2.19	15.66
0.15	30	2	31	1.61	2.21	15.55
0.20	28	2	28	1.55	2.23	16.20
$n=7$						
0.05	29	2	31	1.44	2.23	13.58
0.10	30	2	31	1.44	2.24	13.71
0.15	29	2	31	1.42	2.25	13.84
0.20	29	2	31	1.43	2.26	14.36
$n=10$						
0.05	29	2	31	1.17	2.28	11.78
0.10	30	2	31	1.18	2.29	12.01
0.15	27	2	31	1.18	2.28	12.29
0.20	30	2	31	1.17	2.31	12.59
$n=15$						
0.05	30	2	31	0.82	2.36	10.36
0.10	29	2	31	0.82	2.36	10.51
0.15	30	2	31	0.82	2.37	10.74
0.20	28	2	31	0.82	2.37	11.10

Similar to Table 1, there is a large difference between n_S and n_L. A smaller value of *EARL*$_1$ is shown for a larger *n*. A smaller *W* and a larger *K* are also observed for a larger *n*. Overall, a similar trend is observed for Tables 1 and 2

5 COMPARISON

The proposed chart is compared with the following γ charts: the synthetic-γ, VSS-γ, VSS EWMA-γ^2, EWMA-γ^2 and Shewhart-γ charts.

Table 3 shows the *ARL*$_1$ values of the proposed VSS synthetic-γ chart and the five competing charts, as mentioned in the previous paragraph. The *ARL*$_1$ values are shown for $n \in \{5,7,10,15\}$, $\tau \in \{1.1,1.2,1.5,2.0\}$ and $\gamma_0 = 0.05$, with the *ARL*$_0$ being set as 370.4. To facilitate comparisons, the relative *ARL* (*RARL*), which is the ratio of the *ARL*$_1$ for the competing chart against the *ARL*$_1$ for the VSS synthetic-γ chart, is shown in Table 3. For instance, for *n* = 5 and $\tau = 1.1$, the *RARL* for the Shewhart-γ chart is $\frac{159.86}{68.92} = 2.32$. The proposed chart outperforms competing charts with a *RARL* that is larger than unity.

Table 3: The *ARL*$_1$ for the Shewhart-γ, VSS-γ, EWMA-γ^2, VSS EWMA-γ^2, synthetic-γ, and VSS synthetic-γ charts

τ	Shewhart-γ		VSS-γ		EWMA-γ^2		VSS EWMA-γ^2		Synthetic-γ		VSS synthetic-γ
	n = 5										
	ARL$_1$	*RARL*	*ARL*$_1$	*RARL*	*ARL*$_1$	*RARL*	*ARL*$_1$	*RARL*	*ARL*$_1$	*RARL*	*ARL*$_1$
1.1	159.86	2.32	103.22	1.50	51.03	0.74	30.08	0.44	115.42	1.67	68.92
1.2	64.69	4.51	28.33	1.98	20.38	1.42	11.98	0.84	37.67	2.63	14.34
1.5	10.57	7.19	4.72	3.21	5.76	3.92	4.00	2.72	5.76	3.92	1.47
2.0	2.89	2.89	2.22	2.22	2.36	2.36	2.10	2.10	1.97	1.97	1.00
τ	*n* = 7										
	ARL$_1$	*RARL*	*ARL*$_1$	*RARL*	*ARL*$_1$	*RARL*	*ARL*$_1$	*RARL*	*ARL*$_1$	*RARL*	*ARL*$_1$
1.1	141.22	2.45	88.30	1.53	39.32	0.68	23.66	0.41	97.69	1.70	57.57
1.2	50.26	4.73	23.84	2.24	15.44	1.45	9.49	0.89	27.65	2.60	10.62
1.5	7.21	5.46	3.67	2.78	4.26	3.23	3.12	2.36	3.95	2.99	1.32
2.0	2.05	2.05	1.75	1.75	1.80	1.80	1.71	1.71	1.51	1.51	1.00
τ	*n* = 10										
	ARL$_1$	*RARL*	*ARL*$_1$	*RARL*	*ARL*$_1$	*RARL*	*ARL*$_1$	*RARL*	*ARL*$_1$	*RARL*	*ARL*$_1$

1.1	102.27	2.23	74.43	1.62	30.09	0.66	19.13	0.42	78.87	1.72	45.81
1.2	37.09	4.57	18.43	2.27	11.60	1.43	7.29	0.90	19.24	2.37	8.11
1.5	4.77	3.88	2.90	2.36	3.16	2.57	2.51	2.04	2.71	2.20	1.23
2.0	1.52	1.52	1.41	1.41	1.41	1.41	1.47	1.47	1.22	1.22	1.00
τ	*n* = 15										
	ARL_1	*RARL*	ARL_1	*RARL*	ARL_1	*RARL*	ARL_1	*RARL*	ARL_1	*RARL*	ARL_1
1.1	95.85	2.62	60.49	1.65	22.46	0.61	16.02	0.44	58.48	1.60	36.64
1.2	25.03	4.00	13.85	2.22	8.43	1.35	6.12	0.98	12.24	1.96	6.25
1.5	3.02	2.56	2.20	1.86	2.30	1.95	2.02	1.71	1.86	1.58	1.18
2.0	1.19	1.19	1.17	1.17	1.15	1.15	1.16	1.16	1.07	1.07	1.00

From Table 3, the VSS synthetic-γ chart shows a smaller ARL_1 than the Shewhart-γ, VSS-γ and synthetic-γ charts for all *n* and τ values. The magnitude of improvement is quite large for small values of *n* and τ. In particular, comparison with the synthetic-γ chart shows that the VSS feature results in a significant improvement. For example, for *n* = 5 and $\tau = 1.1$, the ARL_1 = 115.42 for the synthetic-γ chart, while ARL_1 = 68.92 for the VSS synthetic-γ chart. This shows that incorporating the VSS feature results in an improvement of 40.29% in the ARL_1 criterion.

However, the VSS synthetic-γ chart does not outperform the EWMA-γ^2 and VSS EWMA-γ^2 charts for all the shift sizes. With the exception of small shift sizes of $\tau = 1.1$, Table 3 shows that the VSS synthetic-γ chart outperforms the EWMA-γ^2 chart for most cases. This is expected, since the EWMA-γ^2 chart is well-known for its sensitivity to small shifts. However, the VSS synthetic-γ chart is not as complicated as the EWMA-γ^2 chart, which makes it more user-friendly for practitioners. Furthermore, the EWMA-γ^2 chart only shows a better performance for $\tau = 1.1$, while, for other values of τ, the VSS synthetic-γ chart shows a better performance. The VSS synthetic-γ chart outperforms the VSS EWMA-γ^2 chart for moderate and large shift sizes of $\tau = 1.5$ and $\tau = 2.0$, but is inferior to the VSS EWMA-γ^2 chart for $\tau = 1.1$ and $\tau = 1.2$.

Performance in terms of the ARL_1 criterion can only be evaluated if τ is known. Since τ may not be known in practical applications, $EARL_1$ comparisons are also made. Table 4 shows the $EARL_1$ values of the VSS synthetic-γ chart and the five competing charts for $n \in \{5,7,10,15\}$ and $\gamma_0 \in \{0.05, 0.10, 0.15, 0.20\}$. Similar to Table 3, the relative *EARL* (*REARL*) is provided for ease of comparison, where the *REARL* is computed and interpreted in a similar way to the *RARL*.

Table 4: The $EARL_1$ for the Shewhart-γ, VSS-γ, EWMA-γ^2, VSS EWMA-γ^2, synthetic-γ, and VSS synthetic-γ charts

γ_0	Shewhart-γ		VSS-γ		EWMA-γ^2		VSS EWMA-γ^2		Synthetic-γ		VSS synthetic-γ
	n = 5										
	$EARL_1$	*REARL*	$EARL_1$	*REARL*	$EARL_1$	*REARL*	$EARL_1$	*REARL*	$EARL_1$	*REARL*	$EARL_1$
0.05	38.06	2.47	23.16	1.50	15.72	1.02	11.24	0.73	27.18	1.77	15.39
0.10	38.34	2.45	23.25	1.48	15.84	1.01	11.25	0.72	27.39	1.75	15.66
0.15	38.34	2.47	23.38	1.50	16.04	1.03	11.44	0.74	27.74	1.78	15.55
0.20	39.57	2.44	23.63	1.46	16.36	1.01	11.61	0.72	28.25	1.74	16.20
γ_0	*n* = 7										
	$EARL_1$	*REARL*	$EARL_1$	*REARL*	$EARL_1$	*REARL*	$EARL_1$	*REARL*	$EARL_1$	*REARL*	$EARL_1$
0.05	32.12	2.37	19.94	1.47	12.52	0.92	9.00	0.66	22.76	1.68	13.58
0.10	32.41	2.36	20.07	1.46	12.62	0.92	9.00	0.66	22.96	1.67	13.71
0.15	32.90	2.38	20.27	1.46	12.81	0.93	9.20	0.66	23.31	1.68	13.84
0.20	33.62	2.34	20.54	1.43	13.08	0.91	9.32	0.65	23.82	1.66	14.36
γ_0	*n* = 10										
	$EARL_1$	*REARL*	$EARL_1$	*REARL*	$EARL_1$	*REARL*	$EARL_1$	*REARL*	$EARL_1$	*REARL*	$EARL_1$
0.05	26.66	2.26	16.93	1.44	9.89	0.84	7.17	0.61	18.70	1.59	11.78
0.10	26.93	2.24	17.03	1.42	9.98	0.83	7.24	0.60	18.89	1.57	12.01
0.15	27.39	2.23	17.21	1.40	10.14	0.83	7.51	0.61	19.22	1.56	12.29
0.20	28.04	2.23	17.49	1.39	10.37	0.82	7.52	0.60	19.69	1.56	12.59
γ_0	*n* = 15										
	$EARL_1$	*REARL*	$EARL_1$	*REARL*	$EARL_1$	*REARL*	$EARL_1$	*REARL*	$EARL_1$	*REARL*	$EARL_1$

0.05	21.30	2.06	14.31	1.38	7.60	0.73	6.00	0.58	14.73	1.42	10.36
0.10	21.53	2.05	14.34	1.36	7.66	0.73	6.00	0.57	14.90	1.42	10.51
0.15	21.93	2.04	14.43	1.34	7.79	0.73	6.20	0.58	15.19	1.41	10.74
0.20	22.50	2.03	14.60	1.32	7.98	0.72	6.39	0.58	15.59	1.40	11.10

From Table 4, the VSS synthetic-γ chart outperforms the Shewhart-γ, VSS-γ and synthetic-γ charts for all values of n and γ_0 considered in Table 4. This result is consistent with the comparison based on the ARL_1 criterion in Table 3. However, the VSS synthetic-γ chart only slightly outperforms the EWMA-γ^2 chart for n = 5, but does not perform as well as the EWMA-γ^2 chart for cases with $n \in \{7,10,15\}$. By comparison, the VSS EWMA-γ^2 chart outperforms the proposed chart for all values of n and γ_0 considered in Table 4.

6 AN ILLUSTRATIVE EXAMPLE

This section shows the implementation of the VSS synthetic-γ chart with the example by Castagliola *et al*. [8], who have shown that it is not appropriate to use $\bar{X}$ and S control charts to monitor the process owing to an unstable mean and standard deviation. However, Castagliola *et al*. [8] conducted a regression analysis that showed a constant proportionality between the standard deviation and the mean of the process. Thus monitoring γ is a good alternative for this process. This section illustrates the monitoring of this process using the VSS synthetic-γ chart.

Table 5 (left-hand side) shows the sample mean $(\bar{X}_i)$, sample standard deviation (S_i) and sample γ $(\hat{\gamma}_i)$ for the Phase-I data, which consist of m = 30 samples, with size n = 5, where $\hat{\gamma}_i = \frac{S_i}{\bar{X}_i}$.

Table 5: Phase-I and Phase-II data

i	Phase-I			Phase-II				
	$\bar{X}_i$	S_i	$\hat{\gamma}_i$	$n(i)$	$\bar{X}_i$	S_i	$\hat{\gamma}_i$	T_i
1	292.600	2.701	0.00923	2	413.397	3.89	0.00941	0.45548
2	289.000	0.707	0.00245	2	417.426	9.644	0.02310	1.94014
3	291.400	2.073	0.00711	30	415.871	5.949	0.01430	**3.14730**
4	288.000	3.937	0.01367	30	415.777	4.435	0.01067	0.59318
5	290.000	0.707	0.00244	2	417.93	7.805	0.01868	1.56002
6	288.200	1.303	0.00452	2	423.277	7.915	0.01870	1.56189
7	535.400	8.264	0.01544	2	418.865	8.058	0.01924	1.61195
8	518.400	7.224	0.01394	30	414.957	2.107	0.00508	**-4.02142**
9	529.200	9.203	0.01739	30	417.808	4.978	0.01191	1.49900
10	527.000	9.591	0.01820	2	412.646	2.721	0.00659	-0.02961
11	533.600	4.929	0.00924	2	424.2	8.064	0.01901	1.59077
12	439.200	3.114	0.00709	30	414.715	4.168	0.01005	0.12606
13	447.200	2.774	0.00620	2	413.253	4.509	0.01091	0.67587
14	443.400	8.173	0.01843	2	413.459	3.824	0.00925	0.43063
15	434.000	2.549	0.00587	2	422.247	1.63	0.00386	-0.62883
16	436.000	1.224	0.00281	2	416.87	5.941	0.01425	1.09971
17	437.600	2.408	0.00550	2	418.77	7.791	0.01860	1.55250
18	419.600	4.037	0.00962	2	411.295	5.532	0.01345	1.00533
19	422.400	4.159	0.00985	2	413.229	11.899	0.02879	**2.34952**
20	416.800	3.962	0.00951	30	423.45	3.97	0.00937	-0.39779
21	420.400	4.979	0.01184	2	417.444	3.495	0.00837	0.28869
22	421.600	2.302	0.00546	2	416.918	6.67	0.01600	1.29312
23	418.400	4.393	0.01050	2	412.434	7.092	0.01720	1.41662
24	410.400	4.219	0.01028	2	418.307	5.981	0.01430	1.10547
25	449.000	6.204	0.01382	2	422.797	5.151	0.01218	0.84672
26	441.600	3.781	0.00856	2	417.55	1.658	0.00397	-0.60128
27	393.200	6.220	0.01582	2	413.16	7.159	0.01733	1.42959
28	401.800	1.483	0.00369	2	421.391	5.792	0.01374	1.04001
29	412.600	3.049	0.00739	2	413.397	3.89	0.00941	0.45548
30	461.400	7.700	0.01669	2	417.426	9.644	0.02310	1.94014

γ_0 is estimated as

$$\hat{\gamma}_0 = \frac{1}{30}\sum_{i=1}^{30}\hat{\gamma}_i = 0.00975 \approx 0.01. \quad (29)$$

Castagliola *et al*. [8] showed that the Phase-I data are IC. Thus the $\hat{\gamma}_0$ in Equation (29) can be adopted.

Next, Phase-II data, which consist of *m* = 30 samples, are collected, and are shown in Table 5 (right-hand side). Similar to the Phase-I data, the $\bar{X}_i, S_i$ and $\hat{\gamma}_i$ values of the Phase-II samples are also shown. As the transformed statistics T_i in Equation (5) are monitored in the VSS synthetic-γ chart, Table 5 also shows the T_i for each sample.

According to Castagliola *et al*. [8], it is important to detect a shift of 20% in γ. Thus the chart is optimised to detect a shift of $\tau = 1.20$. From the methodology in Section 4, for $n = 5, \gamma_0 = 0.01$ and $\tau = 1.20$, $\left(L^*, n_S^*, n_L^*, W^*, K^*\right) = \left(23, 2, 30, 1.58, 2.17\right)$. From these optimal charting parameters, if $-1.58 < T_i < 1.58$, $n(i+1) = 2$, while if $T_i > 1.58$ or $T_i < -1.58$, $n(i+1) = 30$. The sample size for each sample $n(i)$ is shown in Table 5. Since $K^* = 2.17$, the sample is non-conforming if $T_i > 2.17$ or $T_i < -2.17$. The T_i values in bold in Table 5 are the samples that are non-conforming. If *CRL* $\leq$ 23, the chart will give an OOC signal. Adopting these optimal charting parameters results in $\left(ARL_1, SDRL_1\right) = \left(14.02, 20.16\right)$.

Figure 2 shows the γ sub-chart for the Phase-II data. From Figure 2, we can see that there are three non-conforming samples: samples 3, 8, and 19. From Figure 2, $CRL_1 = 3, CRL_2 = 5$ and $CRL_3 = 11$. Since all the *CRL*s are less than 23, OOC signals will be produced at samples 3, 8, and 19.

Figure 2: The γ sub-chart of the VSS synthetic-γ chart corresponding to the Phase II data

For comparison, this paper will also show the monitoring of the Phase-II data with the synthetic-γ chart without the VSS feature. Similar to the VSS synthetic-γ chart, the synthetic-γ chart is optimised to detect a shift of $\tau = 1.20$, which results in the optimal charting parameters $\left(L^*, LCL^*, UCL^*\right) = \left(39, 0.002217, 0.01942\right)$. Note that, since the synthetic-γ chart adopts fixed sample sizes, there is no need to monitor the transformed statistics T_i. Instead, $\hat{\gamma}_i$ is monitored directly. Figure 3 shows the γ sub-chart for the synthetic-γ chart without the VSS feature.

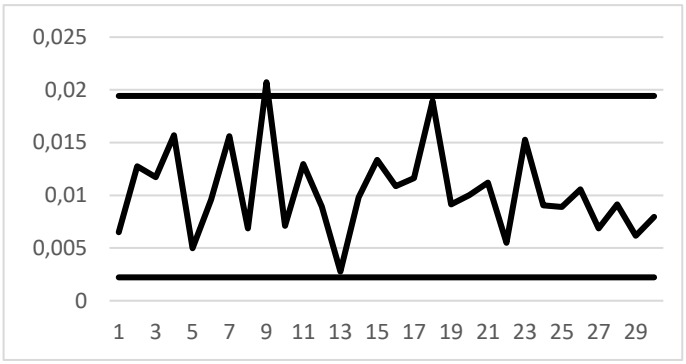

Figure 3: The γ sub-chart of the synthetic-γ chart corresponding to the Phase II data

From Figure 3, only sample 9 is a non-conforming sample, with $CRL_1 = 9$. Thus sample 9 is an OOC sample. This shows that the synthetic-γ chart only managed to detect one OOC sample at sample 9, whereas the VSS synthetic-γ chart detected three OOC samples at samples 3, 8, and 19. This shows that the VSS synthetic-γ chart improves the performance over the synthetic-γ chart.

Figures 2 and 3 can only be obtained if τ is known in advance. Since τ may not be known in advance, we also consider the case when τ is unknown. By adopting the methodology in Section 4 for $n = 5, \gamma_0 = 0.01$ and $(\tau_{\min}, \tau_{\max}) = (1, 2]$, $(L^*, n_S^*, n_L^*, W^*, K^*) = (23, 2, 30, 1.58, 2.17)$ for the VSS synthetic-γ chart, while $(L^*, LCL^*, UCL^*) = (39, 0.002217, 0.01942)$ for the synthetic-γ chart, which are the same optimal charting parameters as those for $\tau = 1.20$. Since the same optimal charting parameters are adopted, the design based on the *EARL* also gives OOC signals for the same samples as the design based on the *ARL*.

7 CONCLUSION

The synthetic-γ chart is attractive to practitioners, as it waits for two successive samples to fall outside the control limits before deciding whether the process is IC or OOC. However, the existing synthetic-γ chart is based on fixed sample sizes, where the same sample size is adopted irrespective of the current sample information. To improve the performance of the existing synthetic-γ chart, a VSS synthetic-γ chart is proposed in this paper to monitor γ. In the proposed chart, the sample size alternates between the small and the large sample sizes, dependent on whether the previous sample is in the central, warning, or non-conforming regions. Formulae to evaluate the *ARL*, *SDRL*, *EARL*, and *ASS* are developed, and optimisation algorithms to obtain the optimal charting parameters are proposed. Tables of optimal charting parameters are also provided to facilitate a quick implementation of the proposed chart. The optimal charting parameters show that there is a large difference between n_S and n_L. Thus practitioners are encouraged to adopt a smaller sample size when $\hat{\gamma}$ is in the central region, and to adopt larger sample sizes when $\hat{\gamma}$ falls in the warning or non-conforming region. The proposed chart shows a significant improvement over the existing synthetic-γ chart. Furthermore, the VSS synthetic-γ chart also outperforms the VSS-γ and Shewhart-γ charts for all shift sizes, while outperforming the EWMA-γ^2 and VSS EWMA-γ^2 charts for moderate and large shift sizes. Note that, with the exception of very small shift sizes, the VSS synthetic-γ chart shows a better performance than the EWMA-γ^2 chart.

8 REFERENCES

[1] **Coelho, M., Chakraborti, S. and Graham, M.A.** 2015. A comparison of Phase I control charts. *The South African Journal of Industrial Engineering*, 26(2), pp. 178-190.

[2] **Teoh, W.L., Fun, M.S., Khoo, M.B.C. and Yeong, W.C.** 2016. Exact run length distribution of the double sampling X-bar chart with estimated process parameters. *The South African Journal of Industrial Engineering*, 27(1), pp. 20-31.

[3] **Kang, C.W., Lee, M.S., Seong, Y.J. and Hawkins, D.M.** 2007. A control chart for the coefficient of variation. *Journal of Quality Technology*, 39(2), pp. 151–158.
[4] **Yeong, W.C., Khoo, M.B.C., Tham, L.K., Teoh, W.L. and Rahim, M.A.** 2017. Monitoring the coefficient of variation using a variable sampling interval EWMA chart. *Journal of Quality Technology*, 49(4), pp. 380–401.
[5] **Calzada, M.E. and Scariano, S.M.** 2013. A synthetic control chart for the coefficient of variation. *Journal of Statistical Computation and Simulation*, 83(5), pp. 853–867.
[6] **Castagliola, P., Celano, G. and Psarakis, S.** 2011. Monitoring the coefficient of variation using EWMA charts. *Journal of Quality Technology*, 43(3), pp. 249–265.
[7] **Castagliola, P., Achouri, A., Taleb, H., Celano, G. and Psarakis, S.** 2013. Monitoring the coefficient of variation using a variable sampling interval control chart. *Quality and Reliability Engineering International*, 29(8), pp. 1135–1149.
[8] **Castagliola, P., Achouri, A., Taleb, H., Celano, G. and Psarakis, S.** 2015. Monitoring the coefficient of variation using a variable sample size control chart. *International Journal of Advanced Manufacturing Technology*, 80, pp. 1561–1576.
[9] **Khaw, K.W., Khoo, M.B.C., Yeong, W.C. and Wu, Z.** 2017. Monitoring the coefficient of variation using a variable sample size and sampling interval control chart. *Communications in Statistics — Simulation and Computation*, 46(7), pp. 5772–5794.
[10] **Yeong, W.C., Lim, S.L., Khoo, M.B.C. and Castagliola, P.** 2018. Monitoring the coefficient of variation using a variable parameters chart. *Quality Engineering*, 30(2), pp. 212–235.
[11] **Anis, N.B.M., Yeong, W.C., Chong, Z.L., Lim, S.L. and Khoo, M.B.C.** 2018. Monitoring the coefficient of variation using a variable sample size EWMA chart. *Computers & Industrial Engineering*, 126, pp. 378-398.
[12] **Reh, W. and Scheffler, B.** 1996. Significance tests and confidence intervals for coefficients of variation. *Computational Statistics & Data Analysis*, 22(4), pp. 449–452.